

Multi-frequency Wiener filtering of CMB data with polarisation

F. R. Bouchet¹, S. Prunet^{1,2}, and Shiv K. Sethi¹

¹, *Institut d'Astrophysique de Paris, CNRS, 98bis Boulevard Arago F-75014 Paris France*

² *Institut d'Astrophysique Spatiale, Bât. 121, 91405 ORSAY, France*

10 October 2018

ABSTRACT

One goal of CMB data analysis is to combine data at different frequencies, angular resolutions, and noise levels in order to best extract the component with a Plankian spectral behaviour. A multi-frequency Wiener filtering method has been proposed in this context by Bouchet, Gispert and Puget (1995) and in parallel by Tegmark and Efstathiou (1996). As shown in Bouchet and Gispert (1998a), this linear method is also convenient to estimate a priori, given a sky model and an experimental description, the residual errors on the CMB power spectrum assuming the foregrounds have been removed with this method. In this paper, we extend the method to the case when additional polarisation data is available. In particular, we derive the errors on the power spectra involving polarisation and show numerical results for the specifications of the future CMB space missions MAP and PLANCK^{*} when it is assumed that the Galactic synchrotron and dust emission are respectively about 40% and 10% polarised. We consider two underlying models for our study: we take a standard CDM model with $\tau = 0.1$ for the extraction of E -mode polarisation and ET cross-correlation; for B -mode polarisation we consider a tilted CDM model with $n_s = 0.9$, $n_T = -0.1$ and $T/S = 0.7$. We find that: (1) The resulting fractional errors on E mode polarisation and TE cross-correlation power spectra are $\lesssim 10$ –30% for $50 \lesssim \ell \lesssim 1000$ for PLANCK. The fractional errors are between 50% to 150% for $\ell \leq 50$, (2) The corresponding fractional errors for MAP are ≥ 300 % for most of the ℓ range, (3) the Wiener filtering give extraction errors ≤ 2 times the expected performance for the combined sensitivity of all the channels of PLANCK. For MAP, the corresponding degradation is $\simeq 4$. (4) if, instead of individual modes, one considers band-power estimates with a logarithmic interval $\Delta\ell/\ell = 0.2$ then the fractional error for MAP drops to $\lesssim 100$ % at the Doppler peak around $\ell \simeq 300$ for the ET signal, and (5) The fractional error for B -mode polarisation detection is $\lesssim 100$ % with PLANCK for $\ell \leq 100$. A band-power estimate with $\Delta\ell/\ell = 0.2$ reduces the fractional errors to $\lesssim 25$ % for $20 \leq \ell \leq 100$.

1 INTRODUCTION

Ever since the detection of CMB temperature anisotropies by the DMR experiment aboard the COBE satellite at angular scales $\geq 7^\circ$ (Smoot *et al.* 1992, Bennett *et al.* 1996), there has been a surge of activity on both theoretical and experimental front. Several detections at smaller angular scales have been reported (for a recent compendium, see Lineweaver and Barbosa 1998). There is great interest in the upcoming satellite projects MAP and PLANCK. These all-sky experiments, it is hoped, will determine the angular power spectrum of CMB temperature fluctuations at all scales greater than a few arc minutes. Various theoretical analyses have shown under fairly general assumptions that this could determine cosmological parameters, Ω , Ω_B , h , etc, with unprecedented precision (Jungman *et al.* 1996, Zaldarriaga *et al.* 1997, Bond *et al.* 1997). In addition, there is growing optimism that these satellite projects might detect

the very small expected signal from the polarised component of the CMB. The information from CMB polarisation could then be combined with temperature signal 1) to check the self-consistency of the predictions of the underlying theoretical model, 2) to further break the degeneracy between some cosmological parameters and 3) to help in unambiguously detecting a tensor-induced component of CMB fluctuations (Seljak & Zaldarriaga 1997, Seljak 1997, Kamionkowski & Kosowski 1997).

A major hurdle in extracting the primary CMB signal from data, apart from noise, is the presence of poorly known Galactic and extra-galactic foregrounds. However, as the foregrounds differ from the CMB emission in both frequency dependence and spatial distribution, one can reduce their level by proper combination of the multi-frequency data of a CMB experiment. Bouchet *et al.* (1995) and Tegmark & Efstathiou (1996) proposed a particular linear scheme, based

on the traditional Wiener filtering method to take full advantage of this fact. The performance of the method has been assessed through detailed numerical simulations performed in the context of the PLANCK preparation (Gispert & Bouchet 1996, Bouchet & Gispert 1998b). It was shown that the residual contamination after cleaning the map is much smaller than the CMB primary signal, and therefore the foregrounds may not be a major obstacle in the extraction of CMB temperature angular power spectrum.

The CMB polarisation signal is expected to be one to two order of magnitudes below the temperature signal. And it is likely to be comparable to the achievable experimental noise in the current experiments. The presence of foregrounds should, of course, make this detection even more difficult. In our Galaxy, the synchrotron emission is highly polarised and would constitute a major foreground for measurements made in the Rayleigh-Jeans part of the CMB spectrum (e.g. MAP and Low-Frequency Instrument -LFI- of PLANCK). The Galactic dust emission is also observed to be polarised and it is the dominant foreground in the Wien part of the CMB spectrum (case of High-Frequency Instrument -HFI- of PLANCK). Prunet *et al.* (1998) modelled and estimated the level of dust polarised emission at high Galactic latitudes, and compared it to the polarised component of the CMB signal. They showed that the scalar-induced polarisation (E-mode) power spectrum and temperature-polarisation cross-correlation are likely to be much larger than the dust polarised emission at high Galactic latitudes. However, the tensor-induced (B-mode) signal is at best comparable to the foreground contamination level. The extraction of such a signal in the presence of comparable instrumental noise, even with small foregrounds, is trickier than the corresponding temperature case, where the signal is much bigger than the instrumental noise.

In this paper, we extend the multi-frequency Wiener filtering method to include the polarisation and temperature-polarisation cross-correlation. The goal of this exercise is to quantify errors in estimating various power spectra when Galactic polarised foregrounds are present. We describe the method in detail in next section. In § 3, we give a description of the polarised foregrounds emission which is used in § 4 to give the resultant errors on the power spectra estimates in the case of MAP and PLANCK. We summarize our results and discuss their limitations and applicability in § 5.

2 MULTI-FREQUENCY WIENER FILTERING ON CMB DATA

We present here an extension of the multi-frequency Wiener filtering technique applied earlier on CMB temperature data (Bouchet *et al.* 1995, Tegmark & Efstathiou 1996, Bouchet & Gispert 1998a, hereafter BG98). The goal of this extension is to see the effect of including polarisation data.

Let us denote the observed data at different frequencies as, y_ν^i , where ν indicates the frequency of the instrumental channel, and i the nature of the observed field (temperature or E -mode polarisation). The B mode polarisation has a vanishing cross-correlation with both T and E and therefore can be treated separately). The E and B modes are the 'divergence' and 'curl' part of the polarisation tensor and are linear combinations of the usual Stoke's parameters

Q and U . The advantage of using these variables is that the B mode polarisation vanishes for scalar-induced perturbations (for details see Seljak 1997). The data points y_ν^i , for a given i , take contributions from various Galactic and extra-galactic sources, apart from the primary CMB signal and instrumental noise. Throughout this paper, we adopt the convention of Tegmark and Efstathiou (1996) and take y_ν^i to mean the 'observed' temperature fluctuation, i.e., the monopole part is first subtracted from the observed surface brightness, which is then divided by $\partial B_0/\partial T_0$, B_0 being the surface brightness of CMB at $T = T_0$. Let us call x_p^j the contribution of the field j due to process p , this is the quantity we want to recover from the observational data y_ν^i . We assume there is a linear relation between them:

$$y_\nu^i = A_{\nu p}^{ij} * x_p^j + b_\nu^i, \quad (1)$$

where $A_{\nu p}^{ij}$ is the instrument response kernel, and b_ν^i is the detector noise level per pixel for the full mission time (all repeated indices are summed over). As discussed in BG98, it is easier to deal with the spherical harmonics transform of Eq. (1), as this non-local equation in pixel space transforms into an algebraic linear equation in multipole space. From now on, all spatially dependent variables are then expressed in multipole space. Eq. (1) translates into:

$$y_\nu^i(l, m) = A_{\nu p}^{ij}(l, m)x_p^j(l, m) + b_\nu^i(l, m) \quad (2)$$

The problem now is to construct an optimal estimator \hat{x}_p^j . We chose this estimator to be linear in the observed data:

$$\hat{x}_p^i = W_{p\nu}^{ij} y_\nu^j. \quad (3)$$

The reconstruction error for a given field and process $(\varepsilon_p^i)^2 \equiv |(\hat{x}_p^i - x_p^i)|^2$ can be written as:

$$\begin{aligned} (\varepsilon_p^i)^2 &= (W_{p\nu}^{ij} A_{\nu p'}^{jk} - \delta_{pp'} \delta_{ik}) (W_{p\nu'}^{il} A_{\nu' p''}^{lm} - \delta_{pp''} \delta_{im}) \langle x_{p'}^k x_{p''}^m \rangle \\ &\quad + W_{p\nu}^{ia} W_{p\nu'}^{ib} \langle b_\nu^a b_{\nu'}^b \rangle; \end{aligned} \quad (4)$$

$W_{p\nu}^{ij}$ is chosen so as to make the variance of the reconstruction error minimal. The derivatives of the error with respect to the filters coefficients $W_{p\mu}^{ic}$ should then be zero. This condition can be expressed as:

$$\begin{aligned} &[(\delta_{jc} \delta_{\mu\nu} A_{\nu p'}^{jk}) (W_{p\nu'}^{il} A_{\nu' p''}^{lm} - \delta_{pp''} \delta_{im}) \\ &\quad + (\delta_{\mu\nu'} \delta_{lc} A_{\nu' p''}^{lm}) (W_{p\nu}^{ij} A_{\nu p'}^{jk} - \delta_{pp'} \delta_{ik})] \langle x_{p'}^k x_{p''}^m \rangle \\ &\quad + (\delta_{\mu\nu} \delta_{ca} W_{p\nu'}^{ib} + \delta_{\mu\nu'} \delta_{cb} W_{p\nu}^{ia}) \langle b_\nu^a b_{\nu'}^b \rangle = 0. \end{aligned} \quad (5)$$

Rearranging terms we get the final equation on the filters:

$$A_{\mu p'}^{ck} W_{p\nu'}^{il} A_{\nu' p''}^{lm} \langle x_{p'}^k x_{p''}^m \rangle + W_{p\nu'}^{ib} \langle b_\nu^c b_{\nu'}^b \rangle = A_{\mu p'}^{ck} \langle x_{p'}^k x_{p'}^i \rangle. \quad (6)$$

2.1 Implementation of foregrounds removal

Eq. (6) is valid for the general case in which various processes, fields, and corresponding instrumental noises could be correlated. We consider here only uncorrelated processes and uncorrelated noises between different fields and channels. We allow for the correlation between the two fields T and E . These conditions can be expressed as:

$$\begin{aligned} \langle x_{p'}^1 x_{p''}^1 \rangle &= \delta_{p' p''} C_{p'}^T = \Delta_{p' p''}^T \\ \langle x_{p'}^1 x_{p''}^2 \rangle &= \delta_{p' p''} C_{p'}^{TE} = \Delta_{p' p''}^{TE} \\ \langle x_{p'}^2 x_{p''}^2 \rangle &= \delta_{p' p''} C_{p'}^E = \Delta_{p' p''}^E \end{aligned} \quad (7)$$

$$\begin{aligned}
 \langle b_{\nu'}^1, b_{\nu'}^1 \rangle &= \delta_{\nu'\nu} B_{\nu'}^T = \mathbf{N}_{\nu'\nu}^T \\
 \langle b_{\nu'}^2, b_{\nu'}^2 \rangle &= \delta_{\nu'\nu} B_{\nu'}^E = \mathbf{N}_{\nu'\nu}^E \\
 \langle b_{\nu'}^1, b_{\nu'}^2 \rangle &= 0
 \end{aligned} \tag{8}$$

With these conditions, Eq. (6) can be written as a system of four matrix equations:

$$\begin{aligned}
 &\mathbf{W}^{11} (\mathbf{A}^{11} \Delta^T \text{tr}(\mathbf{A}^{11}) + \mathbf{N}^T) \\
 + &\mathbf{W}^{12} \mathbf{A}^{22} \Delta^{TE} \text{tr}(\mathbf{A}^{11}) = \Delta^T \text{tr}(\mathbf{A}^{11})
 \end{aligned} \tag{9}$$

$$\begin{aligned}
 &\mathbf{W}^{12} (\mathbf{A}^{22} \Delta^E \text{tr}(\mathbf{A}^{22}) + \mathbf{N}^E) \\
 + &\mathbf{W}^{11} \mathbf{A}^{11} \Delta^{TE} \text{tr}(\mathbf{A}^{22}) = \Delta^{TE} \text{tr}(\mathbf{A}^{22}) \\
 &\mathbf{W}^{21} (\mathbf{A}^{11} \Delta^T \text{tr}(\mathbf{A}^{11}) + \mathbf{N}^T)
 \end{aligned} \tag{10}$$

$$\begin{aligned}
 + &\mathbf{W}^{22} \mathbf{A}^{22} \Delta^{TE} \text{tr}(\mathbf{A}^{11}) = \Delta^{TE} \text{tr}(\mathbf{A}^{11}) \\
 &\mathbf{W}^{22} (\mathbf{A}^{22} \Delta^E \text{tr}(\mathbf{A}^{22}) + \mathbf{N}^E)
 \end{aligned} \tag{11}$$

$$+ \mathbf{W}^{21} \mathbf{A}^{11} \Delta^{TE} \text{tr}(\mathbf{A}^{22}) = \Delta^E \text{tr}(\mathbf{A}^{22}) \tag{12}$$

These equations can be solved by substitution. One can readily verify that the equation for \mathbf{W}^{11} reduces to the form earlier derived by Bouchet *et al.* (1995) and Tegmark & Efstathiou (1996) when the cross-correlation between the fields is switched off.

Bouchet *et al.* (1996) defined a quantity they termed 'quality factor' to quantify the merit of extraction of the signal corresponding to a given process. A straightforward generalization of this quality factor, valid for multiple fields, can be written as:

$$Q_{pp'}^{ij} = \frac{\langle \hat{x}_p^i \hat{x}_{p'}^j \rangle}{\langle x_p^i x_{p'}^j \rangle} = W_{p\nu}^{ik} A_{\nu p'}^{kl} \langle x_p^l x_{p'}^j \rangle \tag{13}$$

where we have used Eq. (6) to write the second equality. Since this is just the ratio of the spectra of the minimum-variance estimated map to the spectra of the real one, it can be viewed as the effective window function of the experiment.

Eq. 13 can be expanded to yield:

$$\mathbf{Q}^{11} = (\Delta^T)^{-1} (\mathbf{W}^{11} \mathbf{A}^{11} \Delta^T + \mathbf{W}^{12} \mathbf{A}^{22} \Delta^{TE}) \tag{14}$$

$$\mathbf{Q}^{22} = (\Delta^E)^{-1} (\mathbf{W}^{21} \mathbf{A}^{11} \Delta^{TE} + \mathbf{W}^{22} \mathbf{A}^{22} \Delta^E) \tag{15}$$

$$\mathbf{Q}^{12} = (\Delta^{TE})^{-1} (\mathbf{W}^{11} \mathbf{A}^{11} \Delta^{TE} + \mathbf{W}^{12} \mathbf{A}^{22} \Delta^E) \tag{16}$$

$$\mathbf{Q}^{21} = \mathbf{Q}^{12} \tag{17}$$

\mathbf{Q}^{11} and \mathbf{Q}^{22} can readily be interpreted as the quality of the reconstruction of temperature and polarisation maps, respectively. As expected in the presence of cross-correlations, the quality factor of either field is better than in the case without cross-correlations. Although the reconstruction of temperature maps is only slightly changed by the cross-correlation term (the term proportional to \mathbf{W}^{12} in Eq. (14)), the quality of the polarisation reconstruction gets a big boost from the presence of temperature-polarisation cross-correlation and almost half the contribution to \mathbf{Q}^{22} comes from the \mathbf{W}^{21} term in Eq. (15). However the meaning of the term \mathbf{Q}^{21} (and \mathbf{Q}^{12}) is not apparent. Much of the contribution to \mathbf{Q}^{12} comes from the term with \mathbf{W}^{11} , and therefore it is very close to the quality factor for the extraction of temperature and is nearly independent of the polarisation noise. It is not surprising as it merely tells us that to optimally reconstruct the cross-correlation one needs to throw out the noisy data, i.e. the polarisation information!

However, the quantity of interest is the error in the extraction of the power spectrum of cross-correlation which should not be confused with \mathbf{Q}^{12} . To get a real idea of the error bars of the different spectra, we must define estimators of those power spectra from the filtered data, and compute their covariances. As we shall see, while \mathbf{Q}^{11} and \mathbf{Q}^{22} directly give the covariance of the E and T power spectra, a more complicated expression is needed for the covariance of the ET power spectrum.

2.2 Unbiased estimators of power spectra

Eq. (3) is the data obtained after performing Wiener filtering on the multi-frequency maps. Our aim in this section is to use this data to write an unbiased estimator of the power spectra, which is defined such that $\langle \hat{C}_p^{ij} \rangle = \langle x_p^i x_p^j \rangle$. From Eqs. (1) and (3), the power spectrum of \hat{x}_p^i can be written as:

$$\langle \hat{x}_p^i \hat{x}_p^j \rangle = W_{p\nu}^{il} W_{p\nu'}^{jm} [A_{\nu p'}^{ln} A_{\nu' p''}^{mq} \langle x_p^n x_p^q \rangle + \langle b_{\nu}^l b_{\nu'}^m \rangle], \tag{18}$$

which can be expressed as:

$$\begin{aligned}
 \langle \hat{x}_p^1 \hat{x}_p^1 \rangle &= (Z_p^{11} C_p^T + b_p^{11}) = Q_p^{11} C_p^T \\
 \langle \hat{x}_p^2 \hat{x}_p^2 \rangle &= (Z_p^{22} C_p^E + b_p^{22}) = Q_p^{22} C_p^E \\
 \langle \hat{x}_p^1 \hat{x}_p^2 \rangle &= (Z_p^{12} C_p^{TE} + b_p^{12}) = Q_p^{12} C_p^{TE}.
 \end{aligned} \tag{19}$$

The meaning of the first equality in Eqs. (19) can be easily understood: the Wiener-filtered power spectrum for a given process can be expressed in terms of the true underlying power spectrum smeared by foregrounds (Z_p^{ij} terms) plus the noise. However, unlike the case with no foregrounds, The 'noise' terms b_p^{ij} have contribution not only from the instrumental noise but also from residual foregrounds from other processes and fields. The second equality comes from Eq. (13). These equations can then be used to write unbiased estimators of the power spectra:

$$\hat{C}_p^T = \frac{1}{Z_p^{11}} \left(\frac{1}{2\ell+1} \sum_m \|\hat{x}_p^1(m) \hat{x}_p^1(m)\| - b_p^{11} \right) \tag{20}$$

$$\hat{C}_p^E = \frac{1}{Z_p^{22}} \left(\frac{1}{2\ell+1} \sum_m \|\hat{x}_p^2(m) \hat{x}_p^2(m)\| - b_p^{22} \right) \tag{21}$$

$$\hat{C}_p^{TE} = \frac{1}{Z_p^{12}} \left(\frac{1}{2\ell+1} \sum_m \|\hat{x}_p^1(m) \hat{x}_p^2(m)\| - b_p^{12} \right) \tag{22}$$

From the unbiased estimators, one can readily compute the covariances of the various power spectra:

$$\mathbf{Cov}(\hat{C}_p^T) = \frac{2}{2\ell+1} (C_p^T Q_p^{11} / Z_p^{11})^2 \tag{23}$$

$$\mathbf{Cov}(\hat{C}_p^E) = \frac{2}{2\ell+1} (C_p^E Q_p^{22} / Z_p^{22})^2 \tag{24}$$

$$\mathbf{Cov}(\hat{C}_p^{TE}) = \frac{1}{2\ell+1} \frac{((Q_p^{12})^2 (C_p^{TE})^2 + Q_p^{11} Q_p^{22} C_p^T C_p^E)}{(Z_p^{12})^2} \tag{25}$$

Given the instrumental noise and the expected level of foregrounds, Eqs. (23), (24), and (25) can be used to estimate the precision with which the power spectra of various quantities can be determined. In the next section, we use the specifications of future experiments MAP and PLANCK to estimate the fractional errors on the power spectra. In calculating the covariances, we have assumed all the processes—

CMB and foregrounds—to be Gaussian. If a fraction of sky, f_{sky} , is covered then the corresponding expressions for the covariances can be obtained by dividing the equations (23), (24), and (25) by f_{sky} . Throughout this paper we assume complete sky coverage, ie. $f_{\text{sky}} = 1$.

3 POLARISED FOREGROUNDS

The most dominant Galactic polarised foregrounds are expected to be the polarised components of synchrotron and dust. In addition, it is possible that the free-free emission is also polarised at 10% level, which could be a further deterrent to extracting the CMB polarisation. We neglect the possibility of polarised free-free emission in this paper (for more details see Keating *et al.* 1997).

The galactic synchrotron radiation originates from the interaction of cosmic ray particles with the galactic magnetic field and is known to dominate the galactic radio emission for frequencies ≤ 10 GHz. In theory, this radiation can be $\simeq 70\%$ polarised, for the observed energy spectrum of the cosmic ray particles (Rybicki & Lightman 1979). However, because of the cancellation due to incoherent addition of polarised component along any line of sight, Faraday depolarisation, and non-uniform magnetic fields, the true polarised percentage is observed to be $\simeq 40\%$ with a dependence on galactic latitude (Burn 1966; Spoetra 1984). The galactic emission in FIR and millimeter wavelengths is dominated by dust emission. The dust particles align themselves with the interstellar magnetic, and because the dust particles are not spherical the resulting FIR and millimeter emission is polarised (Hildebrand & Dragovan 1995).

Polarised dust: The Galactic dust is seen to be polarised at a small level ($\lesssim 10\%$). This is likely to be the major foreground at frequencies at which the PLANCK HFI will operate. Though there exist no observations of polarised dust at high Galactic latitudes, it is possible to model this emission using observations at smaller Galactic latitudes. Prunet *et al.* (1998) modelled this distribution and computed the power spectra of polarisation and temperature-polarisation cross-correlation. They showed that the relevant power spectra can be fitted as:

$$C_E^{\text{dust}}(\ell) = 8.9 \times 10^{-4} \ell^{-1.3} (\mu\text{K})^2 \quad (26)$$

$$C_B^{\text{dust}}(\ell) = 1.0 \times 10^{-3} \ell^{-1.4} (\mu\text{K})^2 \quad (27)$$

$$C_{ET}^{\text{dust}}(\ell) = 1.7 \times 10^{-2} \ell^{-1.95} (\mu\text{K})^2. \quad (28)$$

These power spectra are normalized at 100 GHz. They correspond to Galactic latitudes between 30° and 45° and are taken here as representative of the all sky average (for more details on this and other related issues, see Prunet *et al.* 1998). The dust emissivity is assumed to be proportional to ν^2 with a temperature of 17.5 K (Boulanger *et al.* 1996). For comparison, we recall that the temperature power spectrum at 100 GHz can be fitted by (BG98):

$$C_T^{\text{dust}}(\ell) = 176 \ell^{-3} (\mu\text{K})^2 \quad (29)$$

Polarised Synchrotron emission: This foreground will greatly undermine the performance of MAP and PLANCK LFI in the detection of CMB polarisation. The existing maps of polarised component of Galactic synchrotron shows this emission to be polarised at a level between 20 to 60%,

depending on the Galactic latitude, at radio frequencies ≤ 1.4 GHz (Spoetra 1984). These can be extrapolated to millimeter wavelengths using the frequency dependence of synchrotron emission (Lubin & Smoot 1981). However, such a procedure is fraught with uncertainties: (1) The synchrotron spectrum is not well known up to millimeter frequencies (for recent attempts to measure the spectrum up to 10 GHz see Platania *et al.* 1997), (2) At low frequencies (≤ 1.4 GHz) the polarised emission is not optically thin because of Faraday depolarisation. This means that the observed emission suffers from substantial depolarisation (and also the spatial distribution is affected because of the rotation of the polarisation axis). The Faraday depolarisation is proportional to ν^{-2} and becomes negligible at millimeter wavelengths. Therefore, the degree of polarisation at these frequencies is expected to be higher; in addition it will have a different spatial distribution. So the existing data needs to be corrected for these effects when an extrapolation to higher frequency is performed. It is not easy to do so with the present data. For the lack of data, we assume the synchrotron emission to be polarised at 44% level with the same spatial distribution (ℓ -dependence) as the unpolarised emission. We assume both E and B mode power spectra to correspond to this level of polarisation. It is probably justified because the modelling of dust polarised emission also shows comparable emission for these mode. Furthermore, we assume perfect cross-correlation between E -mode polarisation and temperature. This is likely to be the case because both the polarised and unpolarised emission depend on the square of the magnetic field (its component in the plane of the sky) and the emission at high Galactic latitudes is mostly dominated by one structure. We obtain:

$$C_E^{\text{syn}}(\ell) = 0.2 \times C_T^{\text{syn}}(\ell) \quad (30)$$

$$C_B^{\text{syn}}(\ell) = 0.2 \times C_T^{\text{syn}}(\ell) \quad (31)$$

$$C_{ET}^{\text{syn}}(\ell) = 0.44 \times C_T^{\text{syn}}(\ell) \quad (32)$$

where

$$C_T^{\text{syn}}(\ell) = 4.5 \ell^{-3} (\mu\text{K})^2 \quad (33)$$

at 100 GHz (BG98). One of the aims of taking high level of synchrotron polarised emission and perfect cross-correlations is to consider the 'worst possible' case for the performance of MAP and LFI. This case should be contrasted with the CMB case in which the cross-correlation is $\simeq 1/3$ of the perfect cross-correlation. And therefore the assumed perfect cross-correlation in any foreground means that the total signal is biased in favour of the foreground and would make the extraction of CMB cross-correlation more difficult. However, an important goal is also to ask how well can these foregrounds be extracted using the same experiment that attempts to measure the CMB polarisation. We address this question in a later section. As mentioned above, the free-free emission can also be polarised at a small level but for the assumed level of synchrotron emission it will be sub-dominant to it at all frequencies.

In Fig. 1, we compare the expected CMB E and ET signal with the assumed level of foregrounds. The CMB signal dominates the foregrounds for frequency channels between 44 GHz and 217 GHz. The lower frequency channels of MAP (22 and 30 GHz) and LFI (30 GHz) and the higher frequency

channels of HFI (545 GHz) will be dominated by polarised synchrotron and dust, respectively; these channels will help in an accurate determination of these foregrounds.

Recently, it was argued by Draine and Lazarian (1998) that a part of galactic foreground between 10 and 100 GHz could be contributed by non-thermal emission from rotating dust grains. If this emission is polarized at the same level as we assume in this paper (Eq. 28) then it could add to the polarised galactic emission. However, this emission is subdominant to the polarised synchrotron emission we assume in this paper. And therefore we neglect the effect of spinning dust particles in our discussion in this paper.

Apart from the polarised foreground and in addition to the Galactic unpolarised foregrounds—dust, free-free, and synchrotron—we include several other extragalactic unpolarised foregrounds in our study: The thermal Sunayev-Zeldovitch effect from clusters of galaxies, the infra-red point sources, and the radio point sources (for details see Bouchet & Gispert 1998a). We do not consider any extragalactic polarised foregrounds.

4 EXTRACTION OF POLARISED SIGNAL

Quality factors: As mentioned in the last section, a relevant quantity for determining the merit of signal extraction is the ‘quality factor’ (Eq. (13)). The quality factors for temperature and E -mode polarisation are shown in Figs. (2) and (3) for various processes. It should be noted that in these figures we only show the quality factor for unpolarised synchrotron and dust though we include several other unpolarised Galactic and extragalactic foregrounds in our analysis (see §3). Throughout this and the next subsection, we take the underlying models for calculating various power spectra to be a variant of Λ CDM model with $n_s = 1$, the ratio of scalar to tensor quadrupole $T/S = 0$ (no tensor signal), and the optical depth the last scattering surface $\tau = 0.1$. Finite optical depth to the last scattering surface enhances the polarisation signal for $\ell \lesssim 10$, a part of the spectrum which is of great interest for breaking degeneracies between various cosmological parameters (for details see Zaldarriaga, Spergel, & Seljak 1997). Throughout this paper, we use the CMB Boltzmann code CMBFAST to generate CMB fluctuations (Seljak & Zaldarriaga 1996).

As expected, the temperature signal can be extracted far more cleanly than the polarised signal. The quality factor for the extraction of CMB drops exponentially as the ℓ approaches the effective beam width of the respective experiment. Another noticeable feature in temperature quality factors for various experiments is that the spatial distribution of Galactic dust emission can be discerned almost as well as the CMB signal using PLANCK HFI. This is largely owing to the presence of polarised channel at 545 GHz. The signal at these channels will be dominated by Galactic dust emission; and they have sufficiently low noise levels and high enough angular resolution to allow a good determination of the power spectra of the dust emission up to $\ell \simeq 1000$. This should be contrasted with the extraction of unpolarised synchrotron emission, which is one of the dominant contaminant for $\nu \leq 90$ GHz. Unfortunately neither MAP nor LFI can extract this signal well. It is because (a) it does not dominate the signal at any frequency of either MAP or LFI (b) the

signal is the strongest is the lowest resolution channels, and (c) the unpolarised synchrotron and Galactic free-free emission have very similar spatial distribution (assumed to be the same in this paper) and nearly the same frequency dependence, which makes it difficult to extract either of them.

The oscillating nature of quality factors for CMB polarisation attests to the fact that the signal is barely above the noise level. Another important thing to notice in the figures is the quality of extraction of processes like the polarised component of dust and synchrotron. For HFI, the polarised dust can be extracted better than the CMB for much of the ℓ -range. As in the temperature case, it is possible because of the presence of a polarised channel at 545 GHz. Equivalently, the lowest frequency channels of MAP and LFI serve as templates for polarised synchrotron. It should be noted that the synchrotron polarised component can be extracted much better than its unpolarised counterpart, because, whereas the former dominates all other signals at the lowest frequency channels of MAP and LFI, the latter, as discussed above, doesn’t dominate the total signal at any frequency, at least in our modeling.

We shall see below how the information on quality factor translates into errors on power spectra for various processes.

4.1 Errors on power spectra

We use Eqs. (23), (24), and (25) to estimate the fractional errors in the extraction of the CMB E -mode and TE cross-correlation power spectra. The results are shown in Figs.(4), (5), and (6) for the specification of various experiments. For comparison, we also plot the expected errors using the best channel (90 GHz channel for MAP, 100 GHz channel for LFI, and 143 GHz channel for HFI and full PLANCK) and the combined sensitivity of all the channels of each experiment (Bond *et al.* 1997).

For temperature signal, all the experiments give similar results for $\ell \leq 300$. It is expected as the signal of temperature fluctuation is so much above the noise level for all the experiments in this ℓ -range that additional sensitivity does not lead to additional precision in power spectrum estimation. The only source of error in this ℓ -range is cosmic variance which is obviously independent of the experiment. This information could also be gleaned from the quality factor plots. For $\ell \geq 300$, the extraction of temperature signal depends on the relative beam widths of relevant channels of various experiments. As expected, HFI performs best because it will have channels with $5'$ resolution; it is followed in performance, in that order, by LFI and MAP. It should be noted that the results using Wiener filtering generally lie between the performances of best channel and combined sensitivity.

Unlike the temperature fluctuations, the extraction of polarisation and temperature-polarisation cross-correlation depends sensitively on the pixel noise, as is evident from comparison between fractional errors on these quantities for various experiments. (The sharp spikes in ET plots is not a property of the extraction error but merely indicate that the signal vanishes at these values of ℓ in the underlying theoretical model.) The performances of LFI and HFI are similar for $\ell \lesssim 600$ largely because of comparable polarised sensitivity of the 100 GHz LFI and 143 GHz HFI channels.

For larger ℓ , HFI performs better because of its higher angular resolution. Both these experiments should extract both the E-mode power spectrum and ET cross-correlation to 20–30% precision, i.e. signal-to-noise, $(C_\ell/\sqrt{\text{Cov}(C_\ell)})$, of 4–5, for $50 \lesssim \ell \lesssim 1000$. The signal-to-noise is much smaller at larger scales, apart from cosmic variance, because the CMB signal becomes comparable to both foregrounds and pixel noise. A comparison with the results from the combined sensitivity of all channel shows that the presence of foregrounds degrade the signal extraction by a factor ≤ 2 for much of the ℓ range.

From the figures, it is clear that MAP is hampered not only by foregrounds but also by its sensitivity. If the foregrounds were neglected the combined sensitivity of all its channels might enable a marginal detection of this signal. However, our analysis shows that the presence of foregrounds will degrade this detection by a factor $\simeq 4$, and the resultant fractional errors on E and ET cross-correlation power spectra will be $\geq 300\%$ in most of ℓ -range except $\ell \leq 10$. And therefore it seems unlikely that MAP could give a positive detection of either E and ET signal for *individual* modes.

Band-Power estimates : A way to reduce the 'noise' further is by considering band-power estimates around a given ℓ (see Bond 1996 for relevant definitions). Band power taken over a logarithmic interval of $\Delta\ell/\ell$ results in the reduction of errors by a factor of $\sqrt{\Delta\ell}$ around any ℓ . In Figs (7) and (8), expected 1σ measurements are plotted for various experiments, with band powers taken over a logarithmic interval of 20%, i.e. $\Delta\ell/\ell = 0.2$ for PLANCK HFI and LFI. As is clearly seen in the pictorial representation of these figures, LFI and HFI should make a fairly accurate detection of E and TE power spectra for $\ell \lesssim 750$. For MAP these estimates show that the errors for ET signal drop to $\lesssim 100\%$ near the Doppler peak at $\ell \simeq 300$.

It should be borne in mind that in the absence of any data on the power spectrum of polarised synchrotron we took the synchrotron power spectrum to have the same shape as the temperature power spectrum with 44% polarisation and a perfect cross correlation between E and T . By reducing the level of synchrotron foreground and the ET cross-correlation it should be possible to get lower errors. On the other hand, a higher level of polarised synchrotron should allow a better extraction of synchrotron itself, which might be subtracted using methods other than Wiener filtering. Therefore, there is trade-off between a small and large assumed level of foregrounds: a sub-dominant foreground will give smaller formal errors on the extraction of CMB polarisation but these foregrounds themselves will be elusive, thereby making it harder to quantify the errors; on the other hand, a larger foreground can be detected and probably subtracted more efficiently using, for instance, its non-Gaussian nature. These considerations makes it worthwhile to quantify the errors on foreground extraction.

4.2 Extraction of polarised foregrounds

One of the important goals of future multi-frequency experiments is to *detect* and subtract the foregrounds which hinder the determination of CMB signal. At present one has to extrapolate spectral information on various foregrounds from radio and FIR wavelengths to millimeter and sub-millimeter

wavelengths at which the CMB experiments operate. A similar extrapolation is required on the spatial distribution of foregrounds. For instance, the synchrotron spectrum is determined only for $\nu \lesssim 10$ GHz (Platania *et al.* 1997) while the spatial information is known for angular scales $\geq 0.5^\circ$ from the existing all-sky maps (Haslam *et al.* 1981). While dust maps are available with an angular resolution of $5'$ one needs to extrapolate the dust spectrum from $60 \mu\text{m}$ to millimeter wavelengths for a comparison with the CMB signal (Neugebauer *et al.* 1984). It has been pointed out that such an extrapolation, though useful, might result in large errors in a high-sensitivity CMB experiment (Brandt *et al.* 1994). Therefore, it is of paramount importance to determine the spectrum and spatial distribution of the foregrounds from the same experiment which attempts to measure the CMB anisotropies.

As already pointed out in the discussion on quality factors, polarised foregrounds from dust and synchrotron have a very good chance of being extracted as well as the CMB signal from future experiments. The basic requirement for extracting a process well is that it dominates the total signal at least one frequency of the experiment. Both the future experiments MAP and PLANCK will have frequency channels which fulfill this condition—MAP's two lowest frequency channels, centered at 22 and 30 GHz, and LFI's 30 GHz channel are likely to be dominated by polarised synchrotron; the 545 GHz channel of PLANCK will act as a template for polarised dust. In Figs. (9) and (10) we plot the fractional error on the power spectra of various Galactic polarised foregrounds. The polarised component of dust can be extracted even better than the CMB using HFI because of its 545 GHz channel. Similarly, the presence of the lowest frequency channel on MAP and LFI should enable one to extract the synchrotron signal for $\ell \leq 100$. It should be noticed that for all the experiments the fractional errors on ET cross-correlation are larger than the E power spectrum. It is because the ET cross-correlation of foregrounds is mixed with a relatively large CMB ET cross-correlation signal and therefore does not dominate the total signal as the E -mode foreground polarisation. Another noticeable feature of the figures is that MAP performs as well or even better than LFI and PLANCK in extracting the polarised component of synchrotron. It is because MAP has the lowest frequency channel at 22 GHz. Therefore, despite lower sensitivity, MAP has better frequency coverage at frequencies which are dominated by polarised synchrotron signal.

It should be pointed out that the precision of extraction of a given process depends crucially on the other competing processes. For instance, the unpolarised component of synchrotron cannot be extracted as well the unpolarised component not only because the unpolarised component never dominates the total signal at any frequency but also because it is very difficult to extract it from a comparable level of the free-free signal. Therefore, the quality of extraction of synchrotron polarisation shall depend quite sensitively on the presence of other sources of polarised foreground like polarised free-free emission or the extragalactic radio sources which are seen to be polarised at $\lesssim 20\%$ level (Saikia & Salter 1988). The dust polarised signal, however, is unlikely to be affected as there are no known sources of polarised foregrounds in the high frequency range covered by HFI,

except infra-red point sources which might be polarised but will affect the signal only for $\ell \geq 1000$ (Toffolati *et al.* 1997).

4.3 Detection of B-mode polarisation

An unambiguous way to infer the presence of gravitational waves in the early universe is through the detection of B -mode polarisation (Seljak 1997, Kamionkowski & Kosowsky 1997, Seljak & Zaldarriaga 1997). (Gravitational lensing can generate a B -mode signal from a purely E -mode primary input. However, this signal is weak and peaks around $\ell \simeq 1000$ (Zaldarriaga & Seljak 1998, Bernardeau 1998). We neglect it in this paper.) This signal is much smaller than the E -mode polarisation and is negligible for $\ell \gtrsim 100$, but it is potentially detectable because of the high sensitivity of PLANCK. We plot the fractional errors on this quantity in Fig. (11) for the specifications of PLANCK. The base model is tilted CDM with the scalar index $n_s = 0.9$, the tensor index $n_t = -0.1$, and ratio of tensor to scalar quadrupole $T/S = 0.7$. This signal is barely above the noise level and is comparable to the foreground contamination (Prunet *et al.* 1998). However, Fig. (11) suggests that it might be possible to get a marginal detection with PLANCK at low ℓ .

A noteworthy feature of the B -mode detection is that the Wiener filtering result is quite comparable to the performance of the combined sensitivity of all the channels. This is largely because the B -mode signal does not correlate with any other signal and is therefore free of errors coming from cross-correlations with foregrounds of other fields (T and E). Our results suggest that we expect the answer to lie between the case of best channel and the combined sensitivity of all the channels. With band-power estimates with a 20% logarithmic band, the errors drop to $\leq 25\%$ for $20 \leq \ell \simeq 100$. These are shown in Fig. (12).

Also, as seen in Fig. (11), the B -mode dust polarisation can be extracted with much better precision than the CMB signal. It is because though the CMB B -mode signal is more than an order of magnitude below the E -mode signal, we took them to be comparable for foregrounds. This would mean that the B -mode foregrounds will dominate the signal at most of the frequencies of the future experiments, and therefore can be extracted better than the CMB signal. The synchrotron B -mode signal, however, is seen to be much harder to extract.

5 CONCLUSION AND DISCUSSION

We devised a multi-frequency Wiener filtering method to consider the effect of Galactic polarised foregrounds on the detection of CMB E -mode polarisation and ET cross-correlation using future CMB missions. Our results can be summarized as:

- (i) The foregrounds can be subtracted well enough for the LFI and HFI aboard PLANCK to detect the E and ET signal with signal-to-noise $\simeq 2$ –10 for most of the ℓ -range in $50 \leq \ell \lesssim 1000$.
- (ii) The foregrounds are likely to greatly undermine the performance of MAP. It seems unlikely that MAP could detect either E or ET signal for individual modes. However,

by taking band-power estimates with a 20% logarithmic interval, noise levels reduce sufficiently to allow a marginal detection of the ET signal near $\ell \simeq 300$.

(iii) The power spectra of E -mode polarised dust can be extracted for $\ell \lesssim 1000$ range using PLANCK HFI with signal-to-noise between 1 and 10. The ET cross-correlation of this contaminant can be detected with signal-to-noise ≤ 2 for $100 \leq \ell \leq 1000$. The E -mode power spectrum of polarised synchrotron, on the other hand, can only be determined by either MAP and PLANCK LFI for $\ell \leq 100$. This suggests that *both MAP and PLANCK have a fairly good chance of determining the polarised foregrounds which are expected to hamper their performances in the detection of the CMB polarisation, at least for a small range of ℓ .*

(iv) The B -mode polarisation, which unambiguously establishes the presence of stochastic gravitational waves from the inflationary era, can be detected with signal-to-noise $\simeq 1$ by PLANCK for $\ell \lesssim 100$. However, band-power estimates with a 20% logarithmic band will enable its detection with signal-to-noise $\simeq 2$ –4 for $20 \leq \ell \leq 100$.

Another possible way to detect very small signals (E and ET signal with MAP and B signal with PLANCK) is to image a small fraction of the sky at high Galactic latitudes for longer periods. It is expected that PLANCK will image around 1% of the sky at high Galactic latitudes for periods 5–6 times the all sky average. One advantage of this approach is that foreground level at high Galactic latitudes is much smaller than the all sky average (e.g. dust emission is smaller by nearly a factor of 10 at Galactic latitudes north of 70° as compared to the all sky average we use in this paper). However, this will increase the covariance of power spectra by a factor of $\sqrt{f_{\text{sky}}}$. In light of our results one could ask whether it is preferable to deep-image a part of the sky with small foregrounds or one should decrease the covariance by covering a larger fraction of the sky, albeit with higher foreground levels. It is seen from Figs 5 and 6 that the expected errors on the power spectra of ET and E are, for $\ell \simeq 100$, a factor of 6 more than the best performance of MAP without foregrounds. It might be possible in this case to gain at least a factor of 2 (in addition to sensitivity gained by decrease in pixel noise from longer integration time) by imaging 10% of the sky at higher Galactic latitudes where the foreground level is expected to be much smaller. However, this is not the case for the detection of B -mode polarisation by PLANCK. As seen in Fig 11, Wiener filtering extracts the signal almost as well as one could get using the combined sensitivity of all the channels. This means that if 1% of the sky is integrated for a period $\simeq 5$ times more than the all sky average, the fractional error will only *increase* by a factor of $\simeq 4$ because a decrease in foreground level will not affect the fractional errors.

In going from Eqs. (22) to Eqs. (23), (24), and (25), we assumed the foregrounds to be Gaussian, i.e., the 4-point correlation function was assumed to be expressible as a combination of 2-point functions only. This assumption is erroneous for the foregrounds. The irreducible 4-point function from foregrounds can add to the covariances thereby enhancing the errors. We cannot quantify this increase within the framework of this work. However, as pointed out above some of the frequency channels in the future experiments will be dominated by foregrounds. A direct analysis of these maps

is likely to reveal the non-Gaussian nature of foregrounds, which could then be used to quantify errors on CMB extraction.

Dependence on input model : The results presented in the paper obviously depend on the choice of model chosen for generating the CMB fluctuations. We used a variant of CDM model with reionization for the E and ET extractions. Reionization suppresses anisotropies at small angular scales by $\exp(-2\tau)$, which is not a major effect for $\tau = 0.1$ that we choose. The most important effect of reionization is to generate new polarisation anisotropies at $\ell \simeq 2-30$ depending on the optical depth. In the absence of reionization, the signal will be smaller by more than an order of magnitude for $\ell \lesssim 15$. Therefore, the validity of our results will be very sensitive to the underlying model for $\ell \leq 15$.

The detection of polarisation anisotropies at smaller scales should not depend so much on the choice of model, because most variants of Λ CDM models give comparable level of these anisotropies for $\ell \geq 20$. It should be true unless the optical depth to the large scattering surface is large ($\tau \simeq 1$) or that the large scale anisotropies are dominated by tensor anisotropies. However, the current data for temperature anisotropies already suggest that the first Doppler peak is even higher than predicted by Λ CDM model (Netterfield *et al.* 1997), which rules out the possibility of strong reionization and makes it difficult for the scalar anisotropies to be sub-dominant to contribution from gravitational waves. Therefore, it is safe to conclude that our predictions for $\ell \geq 20$ will not be seriously affected by a change in the underlying model.

For B -mode polarisation we considered a model with tensor to scalar quadrupole ratio $T/S = 0.7$. As mentioned above, this will lower the contribution from scalar modes and therefore will reduce the signal-to-noise for the detection of E -mode polarisation. However, the B -mode signal is roughly proportional to the value of T/S within the framework of inflationary models which require $T/S \simeq -7n_T$. As shown above, the B -mode foregrounds can be subtracted quite efficiently and for this model the signal-to-noise for CMB B -mode signal is $\simeq 2-4$. Therefore, it might be possible to detect a signal with a value as small as $T/S \simeq 0.2-0.3$.

The Wiener filtering method assumes *a priori* knowledge of the power spectra of CMB and foregrounds as well as the frequency dependence of foregrounds. Therefore, the error of extraction using this method does not include the error in evaluating these input quantities. Future experiments will make multi-frequency maps with millions of pixels. This will make it difficult to apply the usual maximum likelihood technique to extract various power spectra. Fast methods for tackling this problem are currently being developed (Oh *et al.* 1998). In future, it should become feasible to quantify errors on the extraction of the power spectra from high resolution multiple frequency maps. It should then be possible to revise our estimates of the errors.

REFERENCES

Bennett, C. L., *et al.* 1996, ApJ, 464, L1
 Bernardeau, F., private communication
 Bond, J. R., Efstathiou, G., & Tegmark, M. 1997, MNRAS, 291,

Bond, J. R. 1996, Observations of Large-Scale Structure in the universe, Ed. Schaeffer, R., Les Houches, Elsevier Science Publishers
 Bouchet, F. R., Gispert, R., & Puget, J.-L. 1995, In "Unveiling the Cosmic Infrared Background", AIP Conference Proceedings 348, Baltimore, Maryland, USA, E. Dwek, editor, pages 255–268
 Bouchet, F. R. & Gispert, R. 1998a, in preparation
 Bouchet, F. R. & Gispert, R. 1998b, in preparation
 Bouchet, F. R., Gispert, R., Boulanger, F. & Puget, J. L. 1996, Proceedings of the 16th Moriond Astrophysics meeting "Microwave Background Anisotropies", Les Arcs, France, Eds. F.R. Bouchet, R. Gispert, B. Guiderdoni, & J. Trần Thanh Vân, Editions Frontières
 Boulanger, F., *et al.* 1996, A & A, 312, 256
 Brandt, W. N., *et al.* 1994, ApJ, 424, 1
 Burn, B. J. 1966, MNRAS, 133, 67
 Draine, B. & Lazarian, A. 1998, ApJ, 494, L19
 R. Gispert & Bouchet, F. R. 1996, Proceedings of the 16th Moriond Astrophysics meeting "Microwave Background Anisotropies", Les Arcs, France, Eds. F.R. Bouchet, R. Gispert, B. Guiderdoni, & J. Trần Thanh Vân, Editions Frontières
 Haslam, C. G. T., *et al.* 1981, A & A, 100, 209
 Hildebrand, R. H. & Dragovan, M. 1995, ApJ, 450, 663
 Jungman, G., Kamionkowski, M., Kosowsky, A., Spergel, D. N. 1996, Phys. Rev. D, 54, 1332
 Kamionkowski, M. & Kosowsky, A. 1997, astro-ph/9705219
 Keating, B., Timbie, P. Polnarev, A., & Steinberger, J. 1997, astro-ph/9710087
 Lineweaver, C. H. & Barbosa, 1998, ApJ, 496, 624L; see also <http://www.sns.ias.edu/~max/cmb/experiments.html>
 Lubin, P. & Smoot, G. 1981, ApJ, 245, 1
 Neugebauer, G. *et al.* 1984, ApJ, 278, L1
 Netterfield, C. B., *et al.* 1997, ApJ, 474, 47
 Oh, S. P., Spergel, D. N., & Hinshaw, G. 1998, astro-ph/9805339
 Platania, P., *et al.* 1997, astro-ph/9707252
 Prunet, S., Sethi, S. K., & Bouchet, F. R., 1998, submitted for publication
 Rybicki, G. B. & Lightman, A. 1979, *Radiative Processes in Astrophysics*, New York, Wiley
 Saikia, D., & Salter, C. 1988, ARA & A, 26, 93
 Seljak, U. 1997, ApJ, 482, 6
 Seljak, U. & Zaldarriaga, M. 1996, ApJ, 488, 1
 Smoot, G., *et al.* 1992, ApJ, 396, L1
 Spoelstra, T. A. T. 1984, A & A, 135, 238
 Tegmark, M. & Efstathiou 1996, MNRAS, 281, 1297
 Toffolatti, L., *et al.* 1997, MNRAS, in press (astro-ph/9711085)
 Zaldarriaga, M. & Seljak, U. 1998, astro-ph/9803150
 Zaldarriaga, M., Spergel, D. N., Seljak, U. 1997, ApJ, 488, 1
 Seljak, U. & Zaldarriaga, M. 1997, Phy. Rev. Lett. 78, 2054

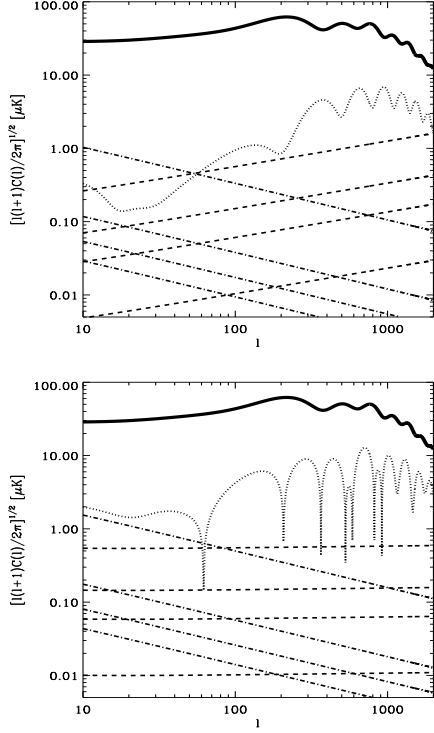


Figure 1. *First Panel* : The power spectrum of the expected E -mode CMB signal is shown along with the dust and synchrotron polarised foregrounds at different frequencies. The *dotted* line show the CMB E -mode power spectra. The *dashed* lines correspond to dust polarised emission (Eq. (28)) while the *dot-dashed* curves correspond to polarised synchrotron (Eq. (32)). The four lines for foregrounds give the expected level of contamination at 44 GHz, 100 GHz, 143 GHz and 217 GHz. The corresponding curves at these frequencies go from top to bottom (bottom to top) for synchrotron (dust) as the frequency is increased. The *thick solid* line gives the temperature power spectrum for the same underlying model, which is taken to be Λ CDM with $\tau = 0.1$. *Second Panel* : Same as the First Panel for ET cross-correlations.

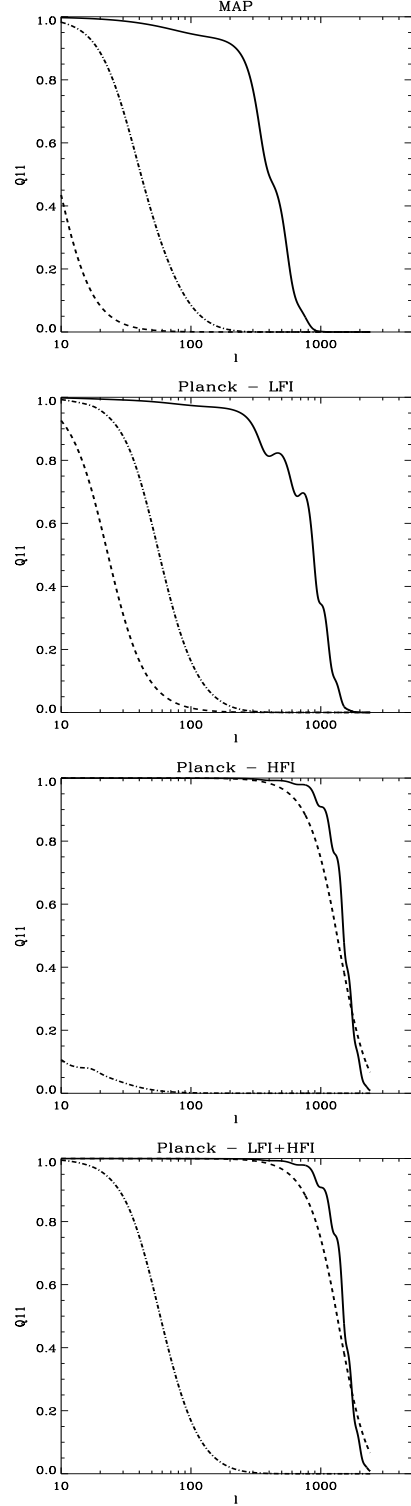


Figure 2. Quality factors for the temperature fluctuations. *Solid*, *dashed*, and *dot-dashed* lines stand for CMB, dust and synchrotron respectively. As can be seen by comparing the effective windows in the case of different experiments, despite its lower sensitivity MAP does as well as the LFI at recovering the synchrotron emission because of its larger frequency coverage; but since this emission is relatively weak, the LFI CMB transmission is better. Also note the improvement on the foreground recovery when the LFI and HFI are combined, although the CMB recovery is not improved by adding the LFI data.

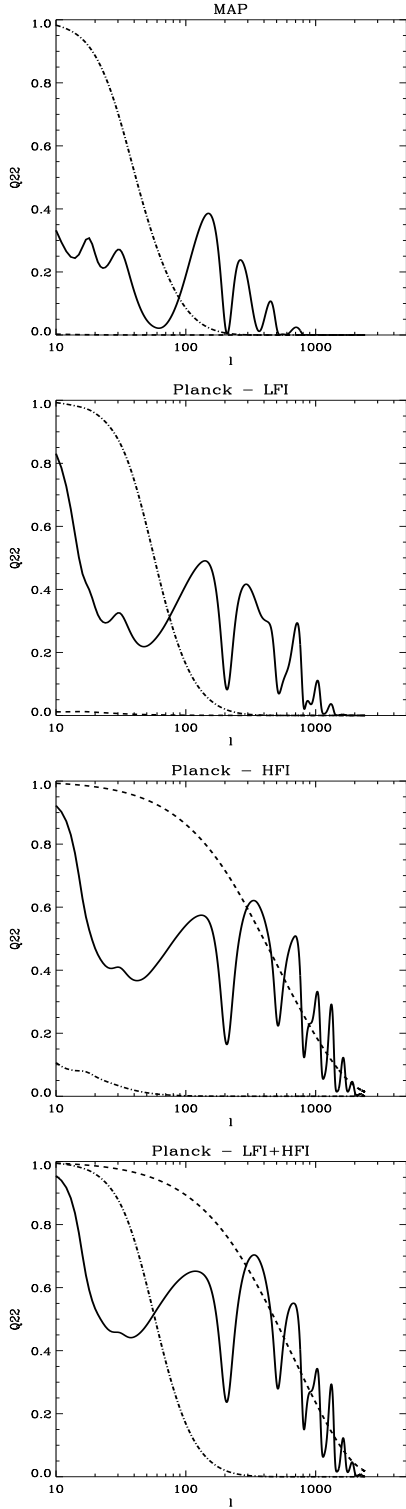


Figure 3. Quality factors for the E -mode polarisation. *Solid*, *dashed*, and *dot-dashed* lines stand for CMB, dust and synchrotron respectively. Note that all the experiments extract the foregrounds better than the CMB for small ℓ . PLANCK HFI extracts the polarised dust better than the CMB at almost all ℓ . This suggests that polarised foregrounds are likely to be extracted as well or better than the CMB. Though this is partly due to our assumed level of foregrounds, this feature reflects the frequency coverage of these experiments

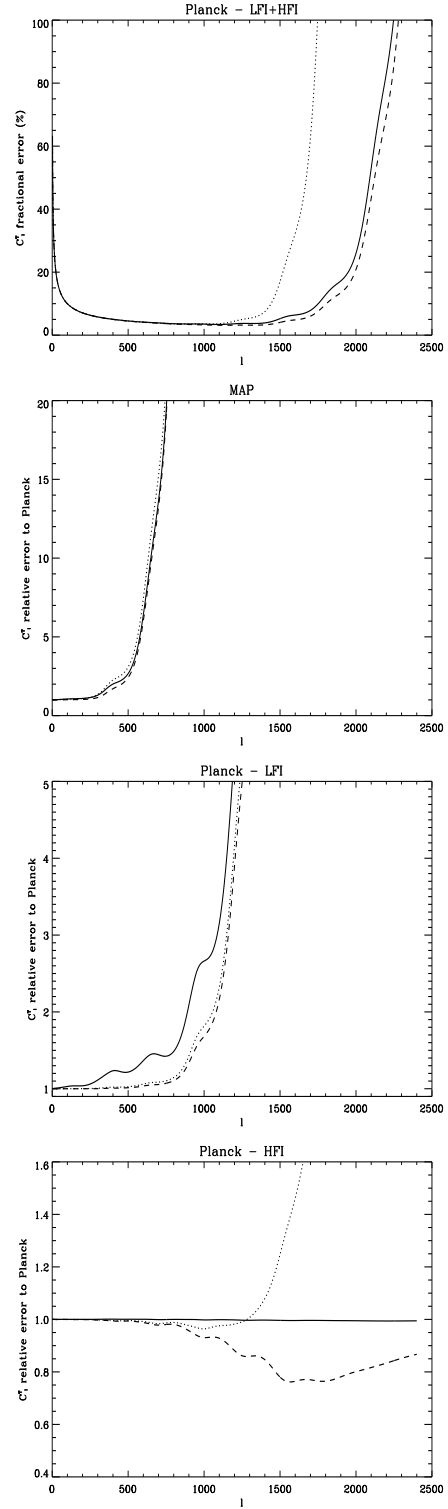


Figure 4. Relative fractional error on temperature power spectra. The first panel shows the expected performance of the full PLANCK mission in extracting this signal. The *Solid* line illustrates the Wiener filtering case, *i.e.* the foregrounds are included and subtracted using the Wiener filtering method described in the text. The *dotted* line corresponds to the case if the signal is extracted using only the best channel of PLANCK (143 GHz) neglecting all the foregrounds. The other panels show the performance of other experiments relative to the PLANCK-Wiener case (the *solid* line in the first panel). In addition to the Wiener and best channel case (the same line style as the first panel), we also show the errors using the combined sensitivity of all the channels (*dashed* line) for various experiments in the last three panels

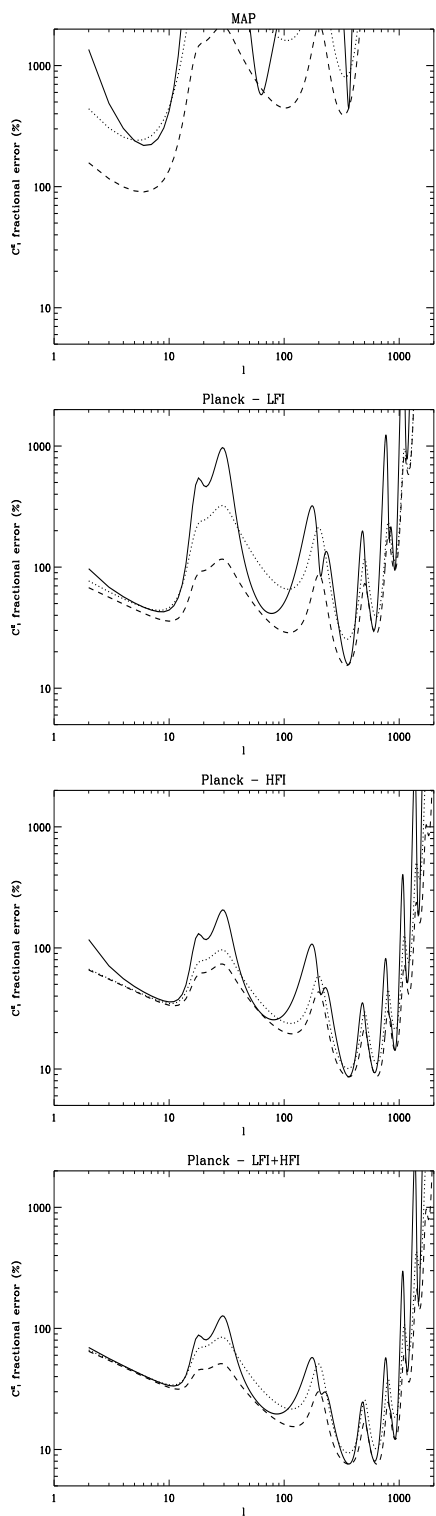


Figure 5. Fractional errors in extracting the E mode polarisation. The *solid*, *dotted*, and *dashed* lines correspond to the expected performances of Wiener filtering, best channel, and combined sensitivity of all the channels of a given experiment, respectively.

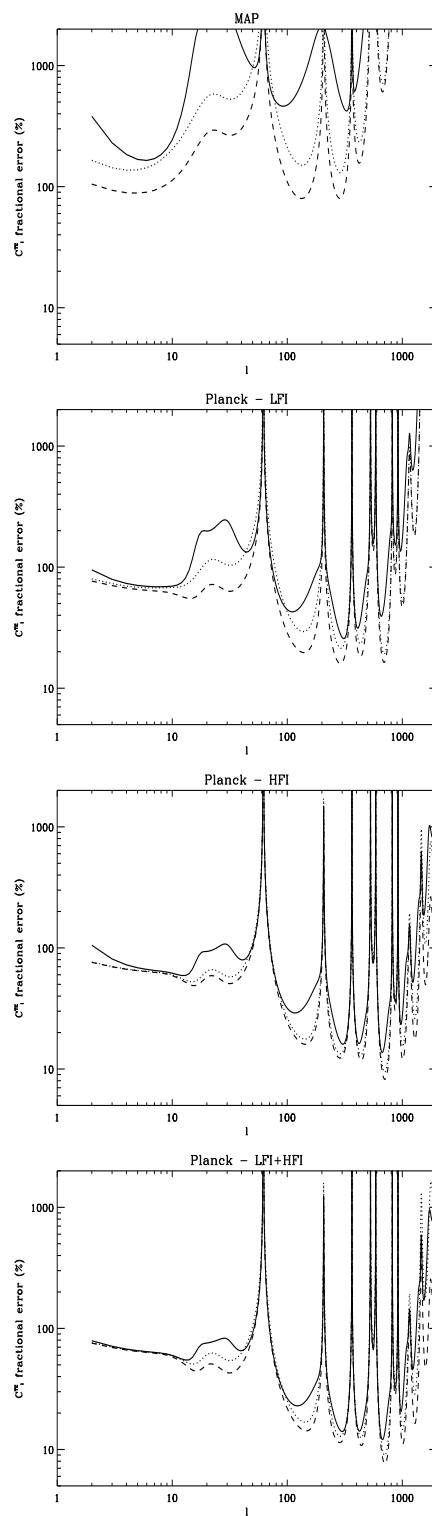


Figure 6. Same as Fig. 5 for the ET cross-correlation. The sharp spikes in the figure merely indicate the values of ℓ at which the signal vanishes.

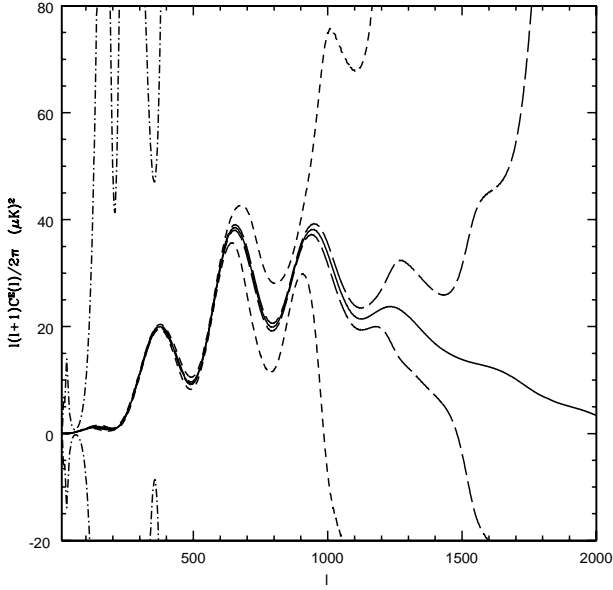


Figure 7. *E*-mode band power estimates. We plot the *E*-mode signal for the underlying model (*solid* line) and show the expected 1σ measurements (*dashed*, *dotted* and *dot-dashed* line for HFI, LFI and MAP respectively) when band power with a logarithmic interval $\Delta\ell/\ell = 0.2$ is taken.

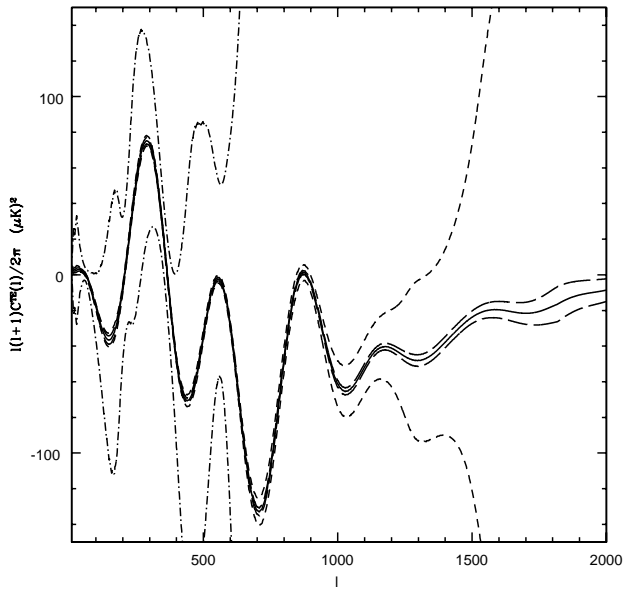


Figure 8. Same as Fig. 7 for the *ET* cross-correlation.

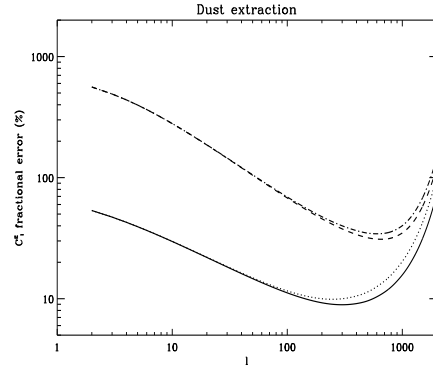


Figure 9. Fractional errors on the extraction of dust *E* and *ET* power spectra with HFI and full PLANCK. The lower two curves correspond to *E* power spectrum (*solid* and *dotted* lines are for HFI and PLANCK respectively) while the upper curves give the errors for *ET* cross-correlation, with the *dashed* line for PLANCK and the *dot-dashed* line for PLANCK HFI.

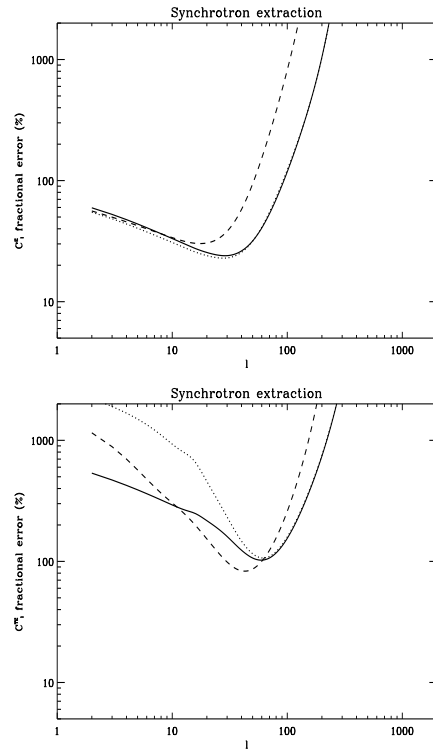


Figure 10. Extraction of synchrotron *E* (Left Panel) and *ET* (Right Panel) power spectra with LFI (*dotted* line), full PLANCK (*solid* line), and MAP (*dashed* line).

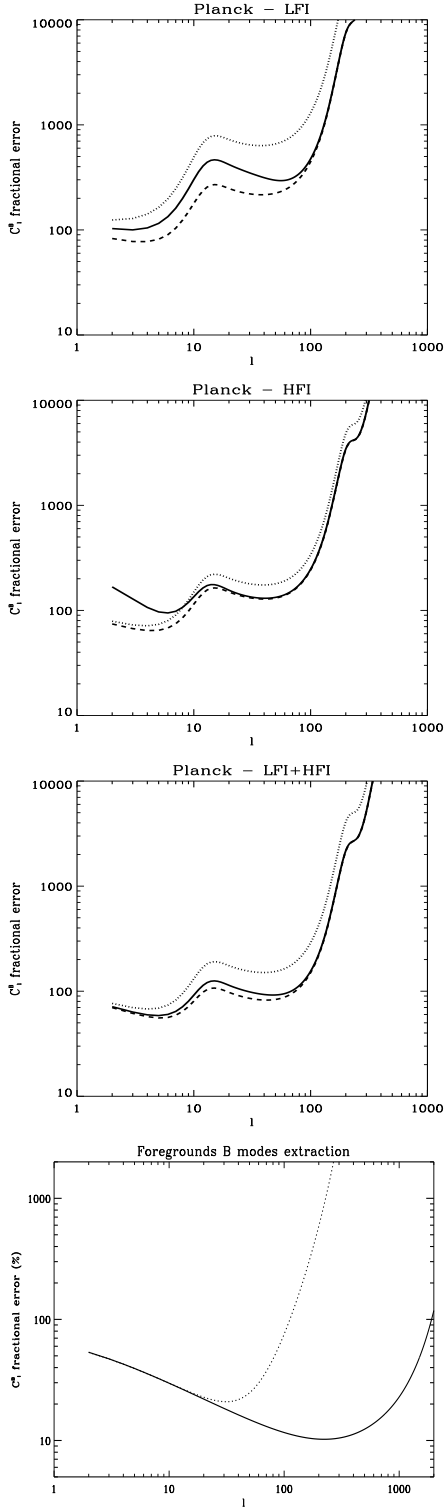


Figure 11. Fractional errors for B -mode polarisation are shown in the first three panels. The *solid*, *dotted*, and *dashed* curves correspond to Wiener, best channel, and combined sensitivity, respectively. The fourth panel shows the corresponding errors in the extraction of the B -mode component of the polarised dust (*solid* line) and synchrotron (*dotted* line). The underlying model was taken to be a Λ CDM model with $n_s = 0.9$, $T/S = 0.7$, and $n_T = 0.1$.

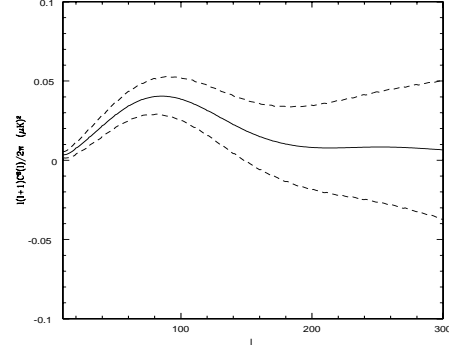


Figure 12. The CMB B -mode signal is plotted along with the expected 1σ measurements with band power taken with a logarithmic interval $\Delta\ell/\ell = 0.2$ for PLANCK.